Published in final edited form as:
Immunity. 2014 March 20; 40(3): 400–413. doi:10.1016/j.immuni.2014.02.004.

Distinct Dendritic Cell Subsets dictate the Fate Decision Between Effector and Memory CD8+ T Cell Differentiation by a CD24 dependent mechanism

Taeg S. Kim[1,3], **Stacey A. Gorski**[1,2], **Steven Hahn**[1], **Kenneth Murphy**[4,5], and **Thomas J. Braciale**[1,2,3,*]

[1]Beirne B. Carter Center for Immunology Research, University of Virginia, Charlottesville, VA 22908, USA.

[2]Department of Microbiology, University of Virginia, Charlottesville, VA 22908, USA.

[3]Department of Pathology, University of Virginia, Charlottesville, VA 22908, USA.

[4]Department of Pathology and Immunology, Washington University School of Medicine, 660 South Euclid Avenue, St. Louis, MO 63110, USA.

[5]HHMI, Washington University School of Medicine, 660 South Euclid Avenue, St. Louis, MO 63110, USA.

Summary

The contribution of different DC subsets to effector and memory $CD8^+$ T cell generation during infection and the mechanism by which DC controls these fate decisions is unclear. Here we demonstrated that the $CD103^+$ and $CD11b^{hi}$ migratory respiratory DC (RDC) subsets after influenza virus infection activated naïve virus-specific $CD8^+$ T cells differentially. $CD103^+$ RDC supported the generation of $CD8^+$ T effectors (Teff), which migrate from lymph nodes to the infected lungs. In contrast, migrant $CD11b^{hi}$ RDC activated $CD8^+$ T cells characteristic of central memory $CD8^+$ cells ($CD8^+$ Tcm) including retention within the draining lymph nodes. $CD103^+$ RDC expressed CD24 at an elevated level, contributing to the propensity of this DC subpopulation to support $CD8^+$ Teff differentiation. Mechanistically, CD24 was shown to regulate $CD8^+$ T cell activation through HMGB1 mediated engagement of T cell RAGE. Thus there is distribution of labor among DC subsets in regulating $CD8^+$ T cell differentiation.

*Corresponding author: Mailing address: Carter Immunology Center, University of Virginia, P.O. Box 801386, Charlottesville, VA 22908 Phone: (434) 924-1219 Fax: (434) 924-1221 tjb2r@virginia.edu.

The authors declare no competing financial interests.

Introduction

Lifelong protective immunity against intracellular pathogens such as viruses requires antigen-specific $CD8^+$ T lymphocytes to undergo several distinct events including clonal expansion, acquisition of effector function, migration to the site of infection and self-renewal (Kaech and Wherry, 2007; Lawrence and Braciale, 2004; Williams and Bevan, 2007). The process of generating $CD8^+$ T effector diversity is fine-tuned by a variety of stimuli such as TCR signaling strength and/or duration, engagement of stimulatory or inhibitory receptors, and local inflammatory stimuli, e.g., innate immune effector cells within secondary lymphoid organs (Haring et al., 2006; Iezzi et al., 1998; Joshi et al., 2007). Integration of these signals within the responding T cells leads to epigenetic modifications regulated by several pairs of transcription factors induced during T cell activation and guides the commitment of naïve T cells into activated cells with distinct functionalities and fates.

Recent analyses suggests that both the strength and duration of in particular IL-2-IL-2R signaling play a critical role in regulating the diversification and fate decision of activated $CD8^+$ T cells into effector T cells ($CD8^+$ Teff) (Kalia et al., 2010; Pipkin et al.). Prolonged IL-2 signaling promotes the development of terminally differentiated short-lived effector cells (SLECs, typically marked by $CD127^{lo}$ $KLRG1^{hi}$), at the expense of effectors possessing self-renewal potential (also known as MPEC, memory precursor effector cell, $CD127^{hi}$ $KLRG1^{lo}$). In addition to IL-2R signaling, inflammatory signals (i.e., IL-12 and type I interferon) promote expression of T-bet and repression of Eomes in the responding $CD8^+$ T cells, resulting in differentiation toward SLEC phenotypes (Curtsinger et al., 2003; Joshi et al., 2007; Takemoto et al., 2006), although it is not known to the extent this process is dependent on IL-2-IL-2R signaling. Similarly, elevated Blimp-1 expression in $CD8^+$ T cells receiving sustained survival signals (i.e., marked by elevated CD25 expression) favors the generation of SLECs by reducing Bcl-6 expression, which in turn represses the acquisition of MPEC phenotype by the responding $CD8^+$ T cells (Crotty et al., 2010; Kallies et al., 2009; Rutishauser et al., 2009). Although dynamic interactions between intrinsic and extrinsic factors fine-tune $CD8^+$ T cell differentiation, the nature and type of signals which instruct the fate decision of naïve $CD8^+$ T lymphocytes and the contribution of the interaction between the responding T cell and one or more antigen-presenting cell (APC) types remains ill defined.

A variety of distinct DC subsets populate the respiratory tract, where they survey the respiratory mucosa and parenchyma for foreign antigens including pathogenic microorganisms (Braciale et al., 2012; de Heer et al., 2005). Upon antigen acquisition and receipt of an activation stimulus, several subsets of lung-resident DCs then migrate into the lung-draining lymph nodes (DLNs), where they present the antigens to naïve (or memory) T cells directed to the specific antigen. These migratory DC subsets include $CD103^+CD11b^{+/-}$ ($CD103^+$) and $CD103^-CD11b^{hi}$ ($CD11b^{hi}$) DCs (Jakubzick et al., 2008; Kim and Braciale, 2009; Sung et al., 2006). During influenza A virus (IAV) infection, the migrant $CD103^+$ and $CD11b^{hi}$ RDC play a primary role in orchestrating the induction of an adaptive immune T cell response (Kim and Braciale, 2009), with migrant $CD103^+$ RDC more potent at stimulating the activation and proliferation of naïve IAV-specific $CD8^+$ T cells *in vitro* than $CD11b^{hi}$ RDC. Furthermore, selective *in vivo* depletion of $CD103^+$ RDC prior to IAV

infection resulted in markedly diminished $CD8^+$ T cell responses in the infected lung (GeurtsvanKessel et al., 2008; Helft et al., 2012). These findings suggested that $CD103^+$ RDC might serve as the primary APC for the induction of $CD8^+$ T cell responses to respiratory virus infection although other evidence implicated migrant $CD11b^{hi}$ RDC subset as the dominant APC for $CD8^+$ T cell priming later in the course of infection i.e., at the peak of IAV replication (Ballesteros-Tato et al., 2010).

Currently, it is unknown whether these two distinct RDC subsets have different (or complementary) roles in dictating the course and outcome of $CD8^+$ T cell differentiation *in vivo* following exposure to a respiratory stimulus such as virus infection. In this report, we sought to determine if the two major subsets of migrant RDC capable of activating naïve $CD8^+$T cells, $CD103^+$ RDC and $CD11b^{hi}$ RDC, differed in their capacity to support $CD8^+$ Teff differentiation in response to IAV infection.

Results

Deficiency in $CD103^+$ RDC resulted in impaired $CD8^+$ Teff accumulation in the lungs but not the DLN

Batf3$^{-/-}$ mice lack lung-resident $CD103^+$ RDC (Figure S1A) and migrant $CD103^+$ RDC do not accumulate in the draining lymph nodes (DLN) of *Batf3*$^{-/-}$ mice following IAV infection [(Edelson et al., 2010; Hildner et al., 2008) and Figures S1B].

As recently reported by Helft et al (Helft et al., 2012) for IAV infected *Batf3*$^{-/-}$ mice, we also observed that the influx of IAV specific $CD8^+$ Teff into the infected lungs over time was markedly impaired in these infected $CD103^+$ RDC-deficient animals both by tetramer staining (Figure 1A) and by $CD8^+$ Teff IFN-γ production (Figure 1B). *Batf3*$^{-/-}$ mice displayed enhanced morbidity (i.e., weight loss, Figure S1C), but no difference in the number and type of lung inflammatory cells (not shown). $CD103^+$ RDC-deficiency had no effect on infectious virus titers or virus clearance (d11 p.i.) (Figure S1D; data not shown).

Unlike the infected lungs, we unexpectedly observed no deficit in the accumulation of IAV specific $CD8^+$ T cells in the DLN of infected $CD103^+$ RDC-deficient mice (Figures 1C and 1D). These findings did not reflect an intrinsic property of *Batf3* deficient T cells as *Batf3*$^{-/-}$ $CD8^+$ Teff accumulated normally in the lungs of reconstituted IAV-infected mixed bone marrow (1:1, WT:*Batf3*$^{-/-}$) chimeric mice (Figure S1E). Furthermore, following transfer of WT naive OVA-specific OT1 cells responding to OT1-IAV infection into *Batf3*$^{-/-}$ mice, exhibited defective $CD8^+$ Teff accumulation in the IAV-infected lungs (and spleen), but normal $CD8^+$ T cell accumulation in the DLN (Figure S1F). Further, the same pattern of defective $CD8^+$ Teff accumulation in the IAV infected lungs with normal $CD8^+$ T cell accumulation in the DLN was observed in Langerin-DTR mice (GeurtsvanKessel et al., 2008) following diptheria toxin (DTx) mediated depletion of $CD103^+$ RDC prior to IAV infection (Figures 1E and 1F). In sum, these results suggested that $CD103^+$ RDC play a prominent role in driving the differentiation of activated $CD8^+$ T cells into lung homing Teff, but were not required for activated $CD8^+$ T cell proliferation in the DLN.

Defective egress of CD8$^+$ Teff from the DLN of infected *Batf3*$^{-/-}$ mice with inefficient activation

These findings suggested that naïve IAV-specific CD8$^+$ T cells stimulated in the CD103$^+$ RDC deficient DLN, activated normally but were unable to efficiently migrate out of the DLN to the infected lungs during the acute phase of infection. We next analyzed the tempo and magnitude of circulating IAV-specific CD8$^+$ T cells in infected WT and *Batf3*$^{-/-}$ mice. IAV-specific blood CD8$^+$ Teff were markedly diminished in infected *Batf3*$^{-/-}$ mice up to d10 p.i. (Figure 2A).

Comparable results were obtained in the blood for transferred responding OT1 cells following infection of WT and *Batf3*$^{-/-}$ recipient mice (Figure S2A)

In view of the above findings it was important to establish that the initial activation and early proliferative expansion of IAV-specific CD8$^+$ T cells in the DLN of infected CD103$^+$ RDC deficient mice was unaffected. To do so, we adoptively transferred CFSE-labeled naïve OT1 CD8$^+$ T cells into WT or *Batf3*$^{-/-}$ recipients and analyzed cell division, total OT1 cell accumulation and viability in the DLN at 3.5 days following IAV infection, i.e., during initial CD8$^+$ T cell activation and proliferation (Lawrence and Braciale, 2004). Unexpectedly, we found that the extent of T cell proliferation (i.e., CFSE dilution) (Figure 2B) as well as the total accumulation of proliferating OT1 cells in the DLN (Figure 2C) was markedly decreased in the DLN of *Batf3*$^{-/-}$ mice. This diminished CD8$^+$ T cell response was not due to accelerated apoptosis of the responding CD8$^+$ T cells in the *Batf3*$^{-/-}$ DLN (Figure S2B). Similar results were obtained OT1 cells in the DLN of CD103$^+$ RDC depleted infected Langerin-DTR mice (data not shown). Also CD8$^+$ Teff in the *Batf3*-deficient infected lungs did not demonstrate accelerated apoptosis (Figure S2C) and active division by lung resident CD8$^+$ Teff was comparable in WT and *Batf3*$^{-/-}$ recipients (Figure S2D).

These results suggested that naïve CD8$^+$ T cells could initially activate and proliferate in the CD103$^+$ RDC deficient DLN but do so suboptimally. The “normal” number of responding CD8$^+$ T cells in the DLN of infected CD103$^+$ RDC-deficient mice at d7 - 8 p.i. (Figures 1C and D) most likely reflects the inability of these responding suboptimally stimulated CD8$^+$ T cells to efficiently egress from the DLN during the acute (effector) phase of the host response to infection, resulting in their progressive accumulation in the DLN. Thus, the stimulation of naïve CD8$^+$ T cells by CD103$^+$ RDC in the DLN may be necessary for the activated proliferating T cells to acquire an essential property of the CD8$^+$ Teff, that is, the capacity to leave the LNs and ultimately home to the site of infection.

Impact of stimulation by CD103$^+$ RDC on the phenotypic profile of CD8$^+$ T effectors

We next examined early T cell activation markers and markers characteristic of developing CD8$^+$ Teff in specific CD8$^+$ T cells (adoptively transferred OT1 cells) responding to IAV-OT1 infection at d3.5 p.i in the DLN of WT or *Batf3*$^{-/-}$ recipients. Wheras expression of early activation markers such as CD44 and CD69 by OT1 cells as well as *ex vivo* antigen triggered T cell IFN-γ expression were comparable in infected WT or *Batf3*$^{-/-}$ recipients, OT1 cells activated in the CD103$^+$ RDC-deficient DLN displayed decreased CD25 and Granzyme B expression and elevated expression of CD62L (Figure 2D and Figure S2E). T cell fate determining transcription factors T-bet and Blimp-1 were likewise decreased in

OT1 cells activated within the DLN of infected *Batf3*$^{-/-}$ recipient mice (Figures 2E and 2F). [Note that the histograms for T-bet and Blimp-1 expression are displayed on a log scale while the bar graphs for MFI are on a linear scale]. A more extensive analysis of a range of markers associated with CD8^{+} Teff (or Tcm) differentiation in CD8^{+} T cells isolated from CD103^{+} RDC sufficient or deficient DLN including elevated CCR5 expression in the activated OT1 cells from WT DLN is shown in Figure S2E.

T-bet, *Blimp-1* and *Granzyme B* (but not *IFN-γ*) transcripts were likewise diminished in d5 p.i. DLN non-tg activated (CD44^{hi}) CD8^{+} T cells compared to control DLN CD44^{hi} CD8^{+} T cells (Figure 2G). These transcripts were expressed comparably in d5 p.i. DLN CD44^{lo} (non-activated) CD8^{+} T cells from WT or *Batf3*$^{-/-}$ donors (Figure 2G). Thus, engagement of naïve CD8^{+} T cells with CD103^{+} RDC APC may be necessary to generate activated T cells with the properties of CD8^{+} Teff or Tem, i.e., transcriptional profile, marker expression, and capacity to migrate from the DLN to inflammation sites.

CD8^{+} T cells activated in the absence of CD103^{+} RDC displayed central memory phenotypes

In contrast to the activated CD8^{+} Teff or Tem-like T cells stimulated by CD103^{+} RDC, the activated CD8^{+} T cells responding in the CD103^{+} RDC-deficient DLN were defective in their migration out of the DLN during the acute phase of infection and displayed properties, i.e., marker profiles, reminiscent of cells destined to become circulating or secondary lymphoid organ (SLO)-resident or homing memory CD8^{+} Tcm. We next analyzed the properties and fate of IAV-specific CD8^{+} T cells present in the circulation of WT or *Batf3*$^{-/-}$ mice following recovery from acute IAV infection. We wanted to determine if the circulating CD8^{+} T cells from *Batf3*$^{-/-}$ mice would largely consist of cells displaying the phenotypic characteristics of CD8^{+} Tcm. Accordingly, the remaining IAV-specific CD8^{+} T cells in recovered WT mice (which had encountered CD103^{+} RDC in the DLN during activation) would therefore be enriched in residual CD8^{+} Teff or Tem-like cells. These Teff or Tem-like cells would in turn gradually diminish in number in the circulation over time along with the fraction of the circulating cells displaying a CD8^{+} Tcm-like memory phenotype.

As Figures 3 A - C demonstrated, circulating IAV-specific CD8^{+} T cells from the blood of recovered *Batf3*$^{-/-}$ mice analyzed at day >60 p.i. contained a large fraction of CD62L^{hi}CCR7^{hi}IL-7R hi cells, consistent with the phenotypic characteristics of CD8^{+} Tcm (Kaech and Wherry, 2007). The corresponding population of circulating Tet^{+}CD8^{+} T cells from recovered WT mice exhibited a lower frequency of CD62L$^{hi/+}$ cells and decreased expression of CCR7 and IL-7Rα as expected for a population of antigen-specific circulating CD8^{+} T cells still relatively enriched for CD8^{+} Teff or Tem. When we analyzed the frequency of Tet^{+}CD8^{+} T cells in the circulation over time (Figure 3D), Ag-specific CD8^{+} T cells from WT mice decreased in frequency gradually as expected during the contraction phase of the host response with loss of CD8^{+} Teff. Circulating Tet^{+}CD8^{+} T cells from the corresponding recovered *Batf3*$^{-/-}$ mice were substantially lower in frequency initially (at d ~20 p.i.) decreased in frequency more slowly over time and were essentially unchanged in

frequency between 40 and 60 days p.i. as expected for a circulating $CD8^+$ Tcm enriched $CD8^+$ T cell population.

Like the acute phase of IAV infection (Figure 1), there were fewer Ag-specific $CD8^+$ T cells present in the lungs of recovered *Batf3*$^{-/-}$ mice than in the WT mice as late as d65 p.i. (Figure 3E). Although the number of Tet^+CD8^+ T cells in the DLN was comparable for recovered $CD103^+$ RDC-sufficient and -deficient mice, the frequency of $CD8^+$ Tcm-like (i.e., $CD62L^{hi}CCR7^{hi}$) cells was greater in the DLN of *Batf3*$^{-/-}$ mice than WT mice (Figure 3F). Ag-specific $CD8^+$ T cells in the DLN of recovered *Batf3*$^{-/-}$ mice were able to orchestrate a $CD8^+$ Teff recall response in the lungs following adoptive transfer into congenic WT ($CD103^+$ RDC containing) recipients and subsequent IAV challenge infection (Figure S3).

$CD11b^{hi}$ RDC are the second major migrant DC populations which can trigger anti-viral naïve $CD8^+$ T cell activation in the DLN (GeurtsvanKessel et al., 2008;Kim, 2009 #145). $CD11b^{hi}$ RDC migrate in normal numbers from the lungs to the DLN of IAV infected *Batf3*$^{-/-}$ mice (Figures S1A and B). We wished to determine if the early activation profile and *in vivo* homing of IAV-specific naïve $CD8^+$ T cells stimulated *in vitro* by $CD103^+$ or $CD11b^{hi}$ RDC respectively mimicked the profile of T cells responding in the WT or *Batf3*$^{-/-}$ DLN *in vivo*, following adoptive transfer of cultured T cells into infected recipients and analysis of the distribution of cells between the infected lungs and the DLN. Accordingly, naïve IAV-specific TCR tg $CD8^+$ T cells were co-cultured with each of these DC populations isolated from the DLN of IAV-infected WT donors at d3 p.i. and analyzed at 4 days of *in vitro* co-culture for cell surface activation marker expression and expression of *T-bet* and *Blimp-1* (Figures S4 A and B). The phenotypic profile of the $CD8^+$ T cells responding to either migrant $CD103^+$ or $CD11b^{hi}$ RDC mirrored the phenotypes of $CD8^+$ T cells responding to IAV infection in the WT or *Batf3*$^{-/-}$

To evaluate the homing capacity of $CD8^+$ T cells activated by the two RDC subsets we adoptively transferred equivalent numbers of the $CD8^+$ T cells stimulated *in vitro* by either $CD103^+$ or $CD11b^{hi}$ migrant RDC into Thy1-mismatched recipient WT mice infected 6 days before with the unrelated IAV B/Lee strain (to exclude the possibility of effects of specific antigen recognition on activated T cell distribution *in vivo*) and analyzed the distribution of the transferred $CD8^+$ T cells within the infected lungs and DLN 24 hours later. We found that naïve T cells stimulated with $CD103^+$ RDC generated activated T cells which preferentially home to the lungs *in vivo* while the $CD8^+$ T cells stimulated by $CD11b^{hi}$ RDC preferentially localize to the DLN (Figure 4 A and B) consistent with the skewing of T cells responding to $CD103^+$ or $CD11b^{hi}$ RDC toward $CD8^+$ Teff or Tem-like and $CD8^+$ Tcm-like activated cells, respectively. Because the number of transferred cells isolated from the respective sites (i.e., lungs or DLN) was low, we modified this strategy to allow amplification of the respective activated $CD8^+$ T cell populations *in vivo*. Briefly, after 4 days of *in vitro* co-culture the activated T cell populations were harvested and again equivalent cell numbers adoptively transferred into uninfected congenic recipient WT mice and the animals rested for 7 days. The recipient mice were then infected with IAV and the accumulation of responding donor $CD8^+$ T cells in the lungs and DLN of infected recipients was evaluated 8 days later. As Figures 4C and 4D demonstrated, $CD8^+$ T cells activated by

either RDC subset trafficked both to the lungs and to the DLN, indicating that both RDC subsets supported Teff- and Tcm-like differentiation. However, as with the cell localization analysis 24 hours after transfer (Figures 4A and B), the responding T cells did so with markedly different efficiency, that is, the $CD8^+$ T cells stimulated by $CD103^+$ RDC preferentially migrated to the infected lungs while the activated T cells stimulated by $CD11b^{hi}$ RDC preferentially targeted to the DLN (Figures 4C and D). Taken together, these findings suggested that $CD103^+$ and $CD11b^{hi}$ RDC supported the differentiation of naïve $CD8^+$ T cells along distinctly different pathways characteristic of Teff and Tcm, respectively.

Costimulatory ligand expression by migrant $CD103^+$ and $CD11b^{hi}$ RDC

Although both $CD103^+$ and $CD11b^{hi}$ RDC can support naïve $CD8^+$ T cell differentiation into Teff or Tem- and Tcm-like cells, we found that the $CD103^+$ RDC were a more potent inducer of $CD8^+$ Teff during the acute phase of the IAV infection. $CD103^+$ RDC appear to be intrinsically more potent APC than $CD11b^{hi}$ RDC when presenting pre-processed peptide antigen (migrant $CD103^+$ and $CD11b^{hi}$ RDC pulsed with synthetic peptide) to naïve $CD8^+$ T cells at a low peptide dose (Figure S4C) (Kim and Braciale, 2009). One explanation at least in part accounting for the intrinsic difference in APC potency is that $CD103^+$ RDC selectively express (or express an elevated level) one or more critical costimulatory ligands which enhance naïve IAV-specific $CD8^+$ T cell activation. The expression of a panel of costimulatory ligand by the two migrant RDC subsets was comparable with the notable exception of the membrane glycoprotein CD24 (Figure 4E). Although expressed by both RDC subsets, CD24 was expressed at ~10 fold higher level by migrant $CD103^+$ RDC than $CD11b^{hi}$ RDC both at the protein level, i.e., cell surface (Figure 4E) and at the mRNA level (Figure 4F). These results raised the possibility that differences in the capacity of $CD103^+$ and $CD11b^{hi}$ RDC to support Teff differentiation may have been linked to cell surface expression of CD24 by these two RDC subsets.

CD24 co-stimulation and RDC dependent $CD8^+$ T cell activation

To interrogate the contribution of CD24 in the activation and initial proliferative response of IAV-specific naïve $CD8^+$ T cells in the DLN, we adoptively transferred naïve OT1 cells prior to infection with IAV-OT1 and evaluated the effect of *in vivo* blockade of CD24 by administration (at d1 and d3 p.i.) of blocking CD24 antibody (Askew and Harding, 2008; Liu et al., 1992) on the early proliferative response and accumulation of responding OT1 cells in the DLN (Figure 5A). CD24 blockade resulted in markedly reduced OT1 cell proliferation and accumulation in the DLN at d4 p.i. (Figure 5B). CD24 blockade likewise resulted in a substantial decrease in the accumulation of IAV-specific endogenous $CD8^+$ Teff in the lungs at d7 p.i. (Figures 5C and 5D) as well as substantially reduced expression of T-bet and Blimp-1 by OT1 cells (Figure S5A) and polyclonal $CD8^+$ Teff (Figures S5 B and C).

Unlike the DLN in infected *Batf3*$^{-/-}$ mice late in infection, *in vivo* CD24 blockade in infected WT mice resulted in a decreased number of IAV-specific $CD8^+$ Teff in the DLN at d7 p.i. (Figure 5E). This finding was not unexpected since both $CD103^+$ and $CD11b^{hi}$ RDC express CD24 and $CD11b^{hi}$ RDC would utilize this costimulatory molecule in the activation

of naïve $CD8^+$ T cells. Indeed, *in vivo* CD24 blockade in infected *Batf3*$^{-/-}$ mice resulted in diminished activation/accumulation of transferred OT1 cells in the DLN at d4 and d7 p.i. (Figures S6 A – D). Furthermore, the *in vitro* proliferation of naïve IAV-specific TCR tg $CD8^+$ T cells in response to either migrant $CD103^+$ or $CD11b^{hi}$ RDC was comparatively inhibited by CD24 blockade (Figure 5F).

In vitro proliferation of naïve $CD8^+$ T cells (to αCD3 and αCD28) was unaffected by CD24 blockade (Figure 6A). However, pre-treatment of IAV-infected BMDC with blocking CD24 antibody prior to i.v. transfer to stimulate a $CD8^+$ T cells *in vivo* resulted in a substantial decrease in the numbers of IAV-specific $CD8^+$ Teff detectable in the d7 responding spleens (Figure 6 B and C).

To directly address whether CD24 expression level by APC affects the magnitude of the *in vivo* $CD8^+$ T cell response, we over-expressed CD24 in WT BMDC using a retrovirus vector (Figures S6E and S6F). We first analyzed the ability of the transduced infected APCs to stimulate a primary $CD8^+$ T cell response *in vivo* following i.v. adoptive transfer. Immunization with CD24 over-expressing infected BMDC markedly enhanced the *in vivo* IAV-specific splenic $CD8^+$ T cell response compared to control vector transduced BMDC (Figure S6G) and the enhanced response was ablated when CD24-tranduced BMDC were pre-treated with anti-CD24 mAb prior to BMDC immunization (Figure S6G).

To determine if, like $CD103^+$ RDC, CD24 over-expressing infected BMDC preferentially drive the activation/differentiation of naïve anti-viral $CD8^+$ T cells into activated cells which preferentially homed to the lungs, we stimulated naïve IAV-specific $CD8^+$ T cells with either infected CD24-tranduced or control vector-transduced BMDC *in vitro* for 4 days as described for RDC (Figures 4A and B) followed by the adoptive transfer of equal number of the activated OT1 cells into IAV-infected recipients with analysis of cell trafficking 24 hours later. Stimulation of the T cells with CD24-transduced BM APC markedly enhanced the localization of the activated T cells to the inflamed lungs compared to vector transduced BMDC (Figure 6D), consistent with $CD103^+$ RDC as APC (Figure 4A and B). This analysis reinforced the view that CD24 can serve as a costimulatory ligand in $CD8^+$ T cell activation and further suggested that the level of CD24 expression by DC APC influenced the subsequent differentiation of activated T cells into Teff–like cells with the capacity to home to sites of inflammation.

CD24 controls naïve $CD8^+$ T cell fate decision via RAGE engagement

Our observations suggest that the level of cell surface expression of the costimulatory molecule CD24 may, in part at least, account for the difference in the ability of $CD103^+$ and $CD11b^{hi}$ migrant RDC to support $CD8^+$ T effector cell differentiation. Among its' several reported functions, CD24 has been demonstrated to serve as a sensor or receptor for molecules exhibiting damage-associated molecular pattern (DAMP) motifs, in particular HMGB1 (Chen et al., 2009). Of note, HMGB1 have been reported to augment T cell activation through engagement of the Receptor for Advanced Glycation End-products (RAGE) on T cells (Chen et al., 2008; He et al., 2013; Moser et al., 2007a).

Because IAV is a lytic virus, during infection the DAMP HMGB1 might be released from damaged and infected cells in the lungs, captured by CD24 on the surface of $CD103^+$ and $CD11b^{hi}$ RDC and then transported by the migrant RDC to the DLN. To test this, we analyzed cell surface HMGB1 expression on $CD103^+$ and $CD11b^{hi}$ RDC in the IAV infected lungs and in the DLN following RDC migration. Like CD24 expression, $CD103^+$ RDC displayed substantially higher levels of cell surface HMGB1 than the $CD11b^{hi}$ RDC both in the infected lungs (Figure 7A) and the DLN following RDC migration, d3 p.i. (Figure 7B). Importantly, the expression of HMGB1 on the total migrant RDC directly paralleled the level of expression of CD24 (Figure 7C), consistent with the earlier finding that CD24 is a prominent receptor for HMGB1 (Chen et al., 2009).

HMGB1 (like CD24) is minimally displayed on $CD8^+$ T cells (Figure S7A) while as reported (Moser et al., 2007a) the RAGE receptor is prominently expressed on naïve $CD8^+$ T cells (Figure S7A). Pretreatment of naïve IAV-specific $CD8^+$ T cells with blocking anti-RAGE antibody prior to co-culture with DC isolated from the DLN at d3 p.i. resulted in significant inhibition of the proliferative response of the IAV-specific T cells (Figure S7B). Comparable to RAGE blockade, pretreatment of the DC with blocking HMGB1 antibody prior to co-culture with naïve IAV-specific $CD8^+$ T cells also substantially inhibited their proliferation (Figure S7B) in the fashion analogous to *in vitro* CD24 blockade (Figure 5F). Also, as for CD24, *in vivo* blockade of HMGB1 during IAV infection by administration of blocking HMGB1 antibody resulted in the decrease in the accumulation of IAV-specific $CD8^+$ T cells in the DLN (Figure 7D) and the lung (data not shown).

To more directly assess the impact of RAGE engagement on the localization of IAV-specific $CD8^+$ T cells *in vivo* following activation, we examine the effect of RAGE blockade in co-cultures between naïve IAV-specific $CD8^+$ T cells and $CD103^+$ RDC from the d3 p.i. DLN on the migration of $CD8^+$ Teff to the lungs and DLN following adoptive transfer into infected recipients. As Figure 7E demonstrated, *in vitro* blockade of RAGE during *in vitro* stimulation of naïve $CD8^+$ T cells by $CD103^+$ RDC resulted in a significant decrease in accumulation of $CD8^+$ Teff in the infected lungs and enhanced accumulation of these Teff in the DLN.

To further confirm the contribution of RAGE engagement in the localization (and likely fate decision) of responding $CD8^+$ T cells, we constructed mixed bone marrow chimeras (1:1) between WT and RAGE-deficient ($Ager^{-/-}$) donors. Following reconstitution and IAV infection, responding $Ager^{-/-}$ $CD8^+$ T cells were reduced significantly in their accumulation in the infected lungs compared to WT T cells with only a modest, but not statistically significant, reduction in the frequency of responding $Ager^{-/-}$ $CD8^+$ Teff in the DLN (Figure 7F). Taken together, these results indicated that CD24 displayed by RDC acts as a costimulatory ligand, at least in part, through the capture of the alarmin HMGB1 (most likely within the infected lungs) and CD24 mediated its costimulatory effect by HMGB1 dependent engagement of RAGE on $CD8^+$ T cells.

Discussion

Two distinct subsets of migratory respiratory dendritic cells, $CD103^+$ RDC and $CD11b^{hi}$ RDC, serve as potent APC triggering the activation of naïve $CD8^+$ T cells in the DLN. In this report, we provide evidence that during natural infection with IAV the activated $CD8^+$ T cells stimulated following encounter with these two RDC subsets in the DLN in large measure exhibited distinctly different properties. IAV-specific naïve $CD8^+$ T cells stimulated by $CD103^+$ RDC primarily gave rise to activated T cells, which efficiently exited from the DLN during the acute phase of infection and trafficked to the site of IAV infection to carry out effector functions. These activated Teff expressed relatively high levels of the transcriptional regulators, T-bet and Blimp-1, and display certain cell surface markers, e.g. $CD25^{hi}$, $CD62L^{lo}$ and $CCR5^{hi}$, characteristics of $CD8^+$ Teff or Tem. By contrast, those triggered by $CD11b^{hi}$ RDC gave rise to activated T cells that did not efficiently egress from the DLN and consequently were only modestly represented in the IAV-infected respiratory tract during the acute phase of infection (i.e., up to d10 p.i.). Instead, these cells accumulated in the DLN over this time frame. These activated T cells expressed lower levels of the transcriptional regulators, T-bet and Blimp-1, and display cell surface markers, e.g., $CD25^{lo}$, $CD62L^{hi}$, IL-7R#x03B1;^{hi}, reminiscent of activated cells destined to become memory $CD8^+$ T cells, in particular Tcm. We also provide evidence that the costimulatory molecule CD24, which is differentially displayed on the surface of these two RDC subsets, was one important factor in facilitating the differentiation of naïve $CD8^+$ T cells into effector-like or memory-like $CD8^+$ T cells. Our results further suggested that CD24 differentially displayed on the surface of these two DC subsets carried out its costimulatory function by presenting HMGB1 to RAGE on the responding T cells. Thus, CD24 displayed by DC APC through its interaction with RAGE on $CD8^+$ T cells contributed to the fate decision of the responding $CD8^+$ T cells.

DC subsets with different intrinsic properties have been implicated (along with cytokine milieu) as critical in dictating the outcome of naïve T cell differentiation i.e., generation of various Teff subsets and/or the transition into memory (Belz et al., 2002; Sallusto and Lanzavecchia, 2000). More recent studies analyzing the fate decision of naïve $CD8^+$ T cells following antigenic stimulation, i.e., effector cell vs memory cell differentiation, have focused on the duration and/or strength of the initial antigenic stimulus provided by the APC, i.e., the summation of signals emanating both from TCR engagement and co-receptor-ligand interactions (Haring et al., 2006; Iezzi et al., 1998; Joshi et al., 2007). Accordingly, the greater the strength and/or duration of the antigenic stimulus, the more likely the responding $CD8^+$ T cells will display an effector T cell-like profile including upregulated expression of Blimp-1 and T-bet - two transcriptional regulators critical for the differentiation of naïve $CD8^+$ T cells into short-lived Teff capable of egress from the DLN to sites of infection (Kallies et al., 2009). Our findings confirm and extend these earlier results and suggests that the fate decision for naïve $CD8^+$ T cell differentiation into effector or memory phenotype cells, in part at least, resides in the properties of the distinct DC subsets acting as APC with the potent stimulus provided by the $CD24^{hi}$ $CD103^+$ RDC supporting Teff differentiation and the weaker stimulus provided by the $CD24^{low}$ $CD11b^{hi}$ RDC driving the formation of Tcm–like cells. However, CD24 expression on $CD11b^{hi}$ RDC

is heterogeneous and a small fraction of $CD11b^{hi}$ RDC are $CD24^{hi}$ (data not shown) perhaps accounting for the small number of lung homing Teff in infected $CD103^+$ RDC-deficient mice.

CD24 is a cell surface glycosyl-phosphatidylinositol (GPI)–anchored protein expressed on a variety of cell types notably B lymphocytes (Hardy et al., 1984) and a variety of APCs including DCs (Askew and Harding, 2008; Martinez del Hoyo et al., 2002). CD24 was initially identified as a costimulatory molecule functioning primarily on APC to costimulate T cell activation during antigen-specific T cell responses via a CD28-independent costimulatory pathway (Wu et al., 1998). More recently, CD24 was demonstrated to also serve as a stress sensor or receptor recognizing and binding certain damage-associated molecular patterns (DAMPs), notably HMGB1 (Chen et al., 2009). Our results on the association between HMGB1 and CD24 on RDC both in the lungs and following migration to the DLN are consistent with these earlier findings. More importantly, our findings suggest a confluence of the roles of CD24 as a T cell costimulatory molecule and stress sensor through its ability to bind HMGB1 and deliver this cargo to RAGE on naïve T cells. It should, however, be noted that whereas these findings suggest the importance of the HMGB1-CD24 complex as a regulator of T cell activation, other defined (e.g., HSPs) or suggested (e.g., S100 protein) CD24 DAMP ligands could also contribute to costimulatory effect of CD24. Further, RAGE blockade or deficiency in T cells does not fully recapitulate the impact of $CD103^+$ RDC loss on the response of naïve $CD8^+$ T cells suggesting a role for other T cell DAMP receptors in this fate decision (see below).

Along with CD24, HMGB1 has been reported to interact with several other DAMP sensors including several TLRs and the RAGE. RAGE is expressed on a variety of cell types including DC and T cells (Alexiou et al., 2010). Earlier studies on the role of RAGE in T cell activation demonstrated that RAGE blockade (Dumitriu et al., 2005; Moser et al., 2007b) or RAGE deficiency in T cells (Chen et al., 2008; Moser et al., 2007a) resulted in diminished T cell activation and proliferation. Thus we considered RAGE to be an attractive candidate receptor for the HMGB1-CD24 complex displayed by the migrant RDC. Our findings on the impact of RAGE blockade *in vitro* on the subsequent *in vivo* migration properties of activated $CD8^+$ T cells as well as the diminished migration of RAGE deficient activated $CD8^+$ T cells into the IAV-infected lungs and the mixed bone marrow chimeras point to the importance of RAGE and RAGE engagement by HMGB1 in $CD8^+$ T cell activation and differentiation. However, we cannot exclude a complementary or synergistic role of other sensors, e.g., TLRs, in regulating or augmenting RAGE-mediated HMGB1 dependent signaling events. Also, RAGE deficient mice have been reported to display enhanced resistance to IAV infection (van Zoelen et al., 2009 and unpublished data). This outcome most likely reflects the effect of RAGE deficiency on the response of one or more cell types in the lungs to IAV infection likely resulting in decreased pulmonary inflammation and injury.

In summary, we have explored the function of two distinct DC subsets responding in the respiratory tract to virus infection in the generation and properties (i.e., differentiation) of virus-specific $CD8^+$ T cell induced in response to these specialized APC subsets. Our findings suggest a “division of labor” between these two RDC subsets, which allow them to

balance in kind and in time the nature of the antiviral $CD8^+$ T cell response following their encounter with naïve $CD8^+$ T cells in the DLN. This difference in the function of the two DC subsets reflects a quantitative difference in the level of expression of the CD24-HMGB1 complex on these two DC subsets and the interaction of this complex with RAGE on the responding T cells.

Experimental Procedures

Mice, virus and infection

Female C57BL/6 (B6, H-2^b) and Balb/c (H-2^d) mice ranging from 8 to 12 weeks old were purchased from the National Cancer Institute (Frederick, MD). *Batf3*$^{-/-}$ mice on a 129S6/SvEv background were previously generated (Hildner et al., 2008). *Batf3*$^{-/-}$ mice were backcrossed at least ten generations to the C57BL/6 background prior to use in our experiments. Details of the additional mice employed in this study and viral infection are provided under Supplemental Experimental Procedures. All animal experiments were performed in accordance with protocols approved by the University of Virginia Animal Care and Use Committee.

Antibodies, flow cytometry analysis, and intracelluar staining

Monoclonal antibodies (mAb) were purchased from BD-Biosciences (BD) (San Diego, CA) or eBiosciences (eBio) (San Diego, CA) (unless stated), and clones were described in detail previously (Kim and Braciale, 2009). H-$2D^b$ tetramers were purchased from the Trudeau Institute (Saranac Lake, NY). Anti-mouse CD16/32 used for Fc receptor blocking was isolated and purified in our laboratory. For biotinylated mAbs, samples were incubated with streptavidin (SA)-RPE, SA-APC or SA-APC-Cy7.

In vitro DC:T cell co-cultures, antibody blockade and adoptive transfer

For DC:T cell cultures, 1×10^4 DCs and 1×10^5 T cells were cultured in a volume of 200 ml in round-bottomed 96-well plates (Corning) and incubated at 37 °C for 4 days in RPMI 1640 media supplemented with 10 % heat-inactivated FCS, 1 % Sodium Pyruvate, 2mM L-glucose, 20 mM HEPES, 5 mM b-mercaptoenthanol and 100 mg/ml Gentamycin (all from Invtiogen). Peptide-coated DC were prepared by incubating isolated DC with 1 mM peptide (HA d 533-541, H-2) for 1 hr at 37 °C, followed by 2 × washes to remove any free peptides prior to co-culture with T cells. To interfere ligand/receptor interaction in the DC:T cell coculture, blocking mAbs at a final concentration of 20 μg/ml were included in the media. Monoclonal Abs used are M1/69 (anti-mouse CD24, BioLegend), polyclonal rabbit anti-HMGB1 (Sigma), and polyclonal goat anti-mouse RAGE (R&D Systems). For *in vivo* blockade of HMGB1, αHMGB1 (Sigma) was i.n. instilled (80 ug/mouse) at the indicated days post infection.

Purified splenic naive OT1 or Cl-4 Tg $CD8^+$ cells were labeled with carboxyfluorescein diacetate succinimidyl ester (CFDA-SE; Molecular Probes, Eugene, OR) as previously described (Lawrence and Braciale, 2004). A graded number of CFSE-labeled T cells as indicated were i.v. injected into the tail vein of Thy-mismatched congenic mice (Thy1.2) at indicated time points. Recipient mice were then infected with influenza virus 24 hr later.

Quantitative Real-Time PCR

Total RNA was extracted from tissues using Trizol (Invitrogen), according to the manufacturer's instructions. cDNA was prepared with SuperScript II Reverse Transcriptase (Invitrogen) from 2 μg total RNA using randon hexamers. Real-time PCR was performed in an ABI PRISM cycler (Life Technologies) with a SYBR Green PCR kit from Applied Biosystems (Life Technologies) with the following predesigned primer sets: *Granzyme B*, *T-bet*, *Blimp-1*, and *IFN-γ* (all purchased from Applied Biosystems). Expression levels of evaluated genes were calculated with the comparative ΔCt method, and relative abundance was quantified with the $2^{-\Delta Ct}$ method.

Retroviral Constructs and Transductions

For overexpression of CD24 (HSA), the retroviral vector pMIG-R1 (a kind gift from Dr. Timothy Bender, University of Virginia, VA) was used to construct pMIG CD24-IRES-GFP according to previous descriptions (Fahl et al., 2009). Details of procedures are provided under Supplemental Experimental Procedures.

Statistics

A two-tailed unpaired Student *t* test was used to analyze differences in mean values between groups. These statistical analyses were performed using the GraphPad Prism3 Software Program for Macintosh. Results are expressed as means ± SEM. Values of $P < 0.05$ were considered statistically significant (* = $P < 0.05$, ** = $P < 0.01$, *** = $P < 0.001$, **** = $P < 0.0001$).

Supplementary Material

Refer to Web version on PubMed Central for supplementary material.

Acknowledgments

We thank Barbara Small for excellent technical assistance and members of the Braciale laboratory for insightful comments and helpful discussions. We also would like to thank Drs. V. Engelhard, T. Bender and V. Laubach (University of Virginia, VA) for reagents and technical advice. This study is supported by the National Institutes of Health (R01 AI-15608, U19 AI-83024 and R01 HL - 33391 to T.J.B.).

References

Alexiou P, Chatzopoulou M, Pegklidou K, Demopoulos VJ. RAGE: a multi-ligand receptor unveiling novel insights in health and disease. Current medicinal chemistry. 2010; 17:2232–2252. [PubMed: 20459381]

Askew D, Harding CV. Antigen processing and CD24 expression determine antigen presentation by splenic CD4+ and CD8+ dendritic cells. Immunology. 2008; 123:447–455. [PubMed: 17949418]

Ballesteros-Tato A, Leon B, Lund FE, Randall TD. Temporal changes in dendritic cell subsets, cross-priming and costimulation via CD70 control CD8(+) T cell responses to influenza. Nat Immunol. 2010; 11:216–224. [PubMed: 20098442]

Belz GT, Heath WR, Carbone FR. The role of dendritic cell subsets in selection between tolerance and immunity. Immunol Cell Biol. 2002; 80:463–468. [PubMed: 12225382]

Braciale TJ, Sun J, Kim TS. Regulating the adaptive immune response to respiratory virus infection. Nat Rev Immunol. 2012; 12:295–305. [PubMed: 22402670]

Chen GY, Tang J, Zheng P, Liu Y. CD24 and Siglec-10 selectively repress tissue damage-induced immune responses. Science. 2009; 323:1722–1725. [PubMed: 19264983]

Chen Y, Akirav EM, Chen W, Henegariu O, Moser B, Desai D, Shen JM, Webster JC, Andrews RC, Mjalli AM, et al. RAGE ligation affects T cell activation and controls T cell differentiation. J Immunol. 2008; 181:4272–4278. [PubMed: 18768885]

Crotty S, Johnston RJ, Schoenberger SP. Effectors and memories: Bcl-6 and Blimp-1 in T and B lymphocyte differentiation. Nat Immunol. 2010; 11:114–120. [PubMed: 20084069]

Curtsinger JM, Lins DC, Mescher MF. Signal 3 determines tolerance versus full activation of naive CD8 T cells: dissociating proliferation and development of effector function. J Exp Med. 2003; 197:1141–1151. [PubMed: 12732656]

de Heer HJ, Hammad H, Kool M, Lambrecht BN. Dendritic cell subsets and immune regulation in the lung. Semin Immunol. 2005; 17:295–303. [PubMed: 15967679]

Dumitriu IE, Baruah P, Valentinis B, Voll RE, Herrmann M, Nawroth PP, Arnold B, Bianchi ME, Manfredi AA, Rovere-Querini P. Release of high mobility group box 1 by dendritic cells controls T cell activation via the receptor for advanced glycation end products. J Immunol. 2005; 174:7506–7515. [PubMed: 15944249]

Fahl SP, Crittenden RB, Allman D, Bender TP. c-Myb is required for pro-B cell differentiation. J Immunol. 2009; 183:5582–5592. [PubMed: 19843942]

GeurtsvanKessel CH, Willart MA, van Rijt LS, Muskens F, Kool M, Baas C, Thielemans K, Bennett C, Clausen BE, Hoogsteden HC, et al. Clearance of influenza virus from the lung depends on migratory langerin+CD11b-but not plasmacytoid dendritic cells. J Exp Med. 2008; 205:1621–1634. [PubMed: 18591406]

Hardy RR, Hayakawa K, Parks DR, Herzenberg LA, Herzenberg LA. Murine B cell differentiation lineages. J Exp Med. 1984; 159:1169–1188. [PubMed: 6423764]

Haring JS, Badovinac VP, Harty JT. Inflaming the CD8+ T cell response. Immunity. 2006; 25:19–29. [PubMed: 16860754]

He Y, Zha J, Wang Y, Liu W, Yang X, Yu P. Tissue damage-associated “danger signals” influence T-cell responses that promote the progression of preneoplasia to cancer. Cancer research. 2013; 73:629–639. [PubMed: 23108142]

Helft J, Manicassamy B, Guermonprez P, Hashimoto D, Silvin A, Agudo J, Brown BD, Schmolke M, Miller JC, Leboeuf M, et al. Cross-presenting CD103+ dendritic cells are protected from influenza virus infection. J Clin Invest. 2012; 122:4037–4047. [PubMed: 23041628]

Hildner K, Edelson BT, Purtha WE, Diamond M, Matsushita H, Kohyama M, Calderon B, Schraml BU, Unanue ER, Diamond MS, et al. Batf3 deficiency reveals a critical role for CD8alpha+ dendritic cells in cytotoxic T cell immunity. Science. 2008; 322:1097–1100. [PubMed: 19008445]

Iezzi G, Karjalainen K, Lanzavecchia A. The duration of antigenic stimulation determines the fate of naive and effector T cells. Immunity. 1998; 8:89–95. [PubMed: 9462514]

Jakubzick C, Helft J, Kaplan TJ, Randolph GJ. Optimization of methods to study pulmonary dendritic cell migration reveals distinct capacities of DC subsets to acquire soluble versus particulate antigen. J Immunol Methods. 2008; 337:121–131. [PubMed: 18662693]

Joshi NS, Cui W, Chandele A, Lee HK, Urso DR, Hagman J, Gapin L, Kaech SM. Inflammation directs memory precursor and short-lived effector CD8(+) T cell fates via the graded expression of T-bet transcription factor. Immunity. 2007; 27:281–295. [PubMed: 17723218]

Kaech SM, Wherry EJ. Heterogeneity and cell-fate decisions in effector and memory CD8+ T cell differentiation during viral infection. Immunity. 2007; 27:393–405. [PubMed: 17892848]

Kalia V, Sarkar S, Subramaniam S, Haining WN, Smith KA, Ahmed R. Prolonged interleukin-2Ralpha expression on virus-specific CD8+ T cells favors terminal-effector differentiation in vivo. Immunity. 2010; 32:91–103. [PubMed: 20096608]

Kallies A, Xin A, Belz GT, Nutt SL. Blimp-1 transcription factor is required for the differentiation of effector CD8(+) T cells and memory responses. Immunity. 2009; 31:283–295. [PubMed: 19664942]

Kim TS, Braciale TJ. Respiratory dendritic cell subsets differ in their capacity to support the induction of virus-specific cytotoxic CD8+ T cell responses. PLoS One. 2009; 4:e4204. [PubMed: 19145246]

Lawrence CW, Braciale TJ. Activation, differentiation, and migration of naive virus-specific CD8+ T cells during pulmonary influenza virus infection. J Immunol. 2004; 173:1209–1218. [PubMed: 15240712]

Liu Y, Jones B, Aruffo A, Sullivan KM, Linsley PS, Janeway CA Jr. Heat-stable antigen is a costimulatory molecule for CD4 T cell growth. J Exp Med. 1992; 175:437–445. [PubMed: 1346270]

Martinez del Hoyo G, Martin P, Arias CF, Marin AR, Ardavin C. CD8alpha+ dendritic cells originate from the CD8alpha-dendritic cell subset by a maturation process involving CD8alpha, DEC-205, and CD24 up-regulation. Blood. 2002; 99:999–1004. [PubMed: 11807005]

Moser B, Desai DD, Downie MP, Chen Y, Yan SF, Herold K, Schmidt AM, Clynes R. Receptor for advanced glycation end products expression on T cells contributes to antigen-specific cellular expansion in vivo. J Immunol. 2007a; 179:8051–8058. [PubMed: 18056345]

Moser B, Szabolcs MJ, Ankersmit HJ, Lu Y, Qu W, Weinberg A, Herold KC, Schmidt AM. Blockade of RAGE suppresses alloimmune reactions in vitro and delays allograft rejection in murine heart transplantation. American journal of transplantation : official journal of the American Society of Transplantation and the American Society of Transplant Surgeons. 2007b; 7:293–302.

Pipkin ME, Sacks JA, Cruz-Guilloty F, Lichtenheld MG, Bevan MJ, Rao A. Interleukin-2 and inflammation induce distinct transcriptional programs that promote the differentiation of effector cytolytic T cells. Immunity. 32:79–90. [PubMed: 20096607]

Rutishauser RL, Martins GA, Kalachikov S, Chandele A, Parish IA, Meffre E, Jacob J, Calame K, Kaech SM. Transcriptional repressor Blimp-1 promotes CD8(+) T cell terminal differentiation and represses the acquisition of central memory T cell properties. Immunity. 2009; 31:296–308. [PubMed: 19664941]

Sallusto F, Lanzavecchia A. Understanding dendritic cell and T-lymphocyte traffic through the analysis of chemokine receptor expression. Immunol Rev. 2000; 177:134–140. [PubMed: 11138771]

Sung SS, Fu SM, Rose CE Jr. Gaskin F, Ju ST, Beaty SR. A major lung CD103 (alphaE)-beta7 integrin-positive epithelial dendritic cell population expressing Langerin and tight junction proteins. J Immunol. 2006; 176:2161–2172. [PubMed: 16455972]

Takemoto N, Intlekofer AM, Northrup JT, Wherry EJ, Reiner SL. Cutting Edge: IL-12 inversely regulates T-bet and eomesodermin expression during pathogen-induced CD8+ T cell differentiation. J Immunol. 2006; 177:7515–7519. [PubMed: 17114419]

van Zoelen MA, van der Sluijs KF, Achouiti A, Florquin S, Braun-Pater JM, Yang H, Nawroth PP, Tracey KJ, Bierhaus A, van der Poll T. Receptor for advanced glycation end products is detrimental during influenza A virus pneumonia. Virology. 2009; 391:265–273. [PubMed: 19592063]

Williams MA, Bevan MJ. Effector and memory CTL differentiation. Annu Rev Immunol. 2007; 25:171–192. [PubMed: 17129182]

Wu Y, Zhou Q, Zheng P, Liu Y. CD28-independent induction of T helper cells and immunoglobulin class switches requires costimulation by the heat-stable antigen. J Exp Med. 1998; 187:1151–1156. [PubMed: 9529332]

Highlights

- $CD103^+$ RDC drive $CD8^+$ T cell differentiation into lung homing T effectors
- $CD11b^{hi}$ RDC stimulate $CD8^+$ T cell differentiation into central memory-like effectors
- $CD103^+$ RDC express elevated CD24 compared to $CD11b^{hi}$ RDC
- RDC CD24 modulates $CD8^+$ T cell activation by presenting HMGB1 to T cell RAGE

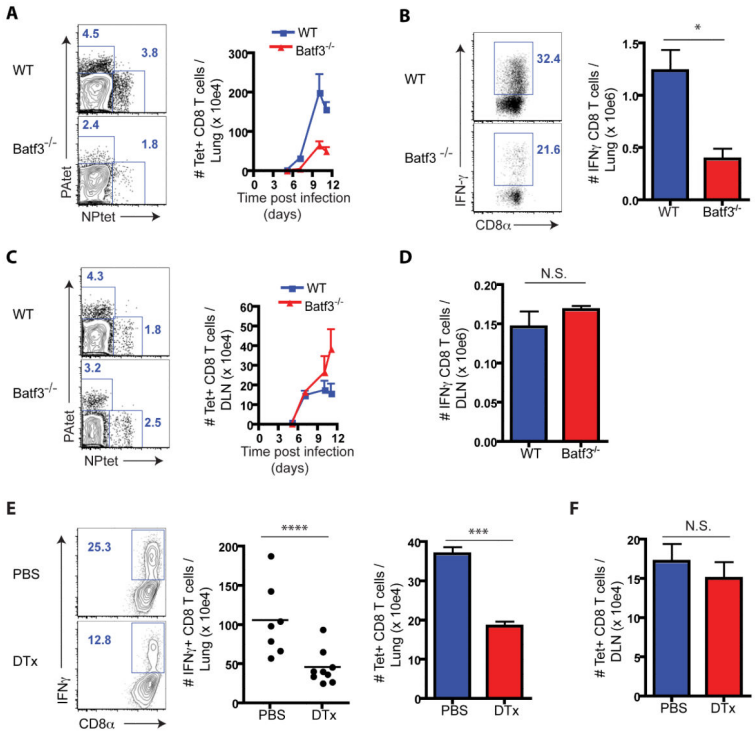

Figure 1.

Deficiency in CD103$^+$ RDC impaired anti-IAV CD8$^+$ Teff accumulation in the lungs, but not DLN. (A – D) *Batf3*$^{-/-}$ and B6 mice were infected with IAV and specific CD8$^+$ T cells in the lungs (A and B) and DLN (C and D) were enumerated over time after tetramer staining. Rep. flow analyses (left panels in A and C) and combined NP- and PA-specific tetramer$^+$ CD8$^+$ T total cell numbers (right panels in A and C) were depicted. (B and D) IFNγ-secreting CD8$^+$ T cells in the infected lung (B) and DLN (D) at d7 p.i. were identified after restimulation with IAV-infected BMDC for 5 hrs *in vitro* (n = 6 - 8 mice/genotype). (E and F) Langerin-DTR mice were depleted of CD103$^+$ RDC by i.n. administration of DTx (or control PBS) followed by IAV infection. At d7 p.i specific CD8$^+$ T cells in the inflamed lung (E) and the responding DLN (F) were enumerated as shown in A and C (n = 7 - 9). See also Figure S1.

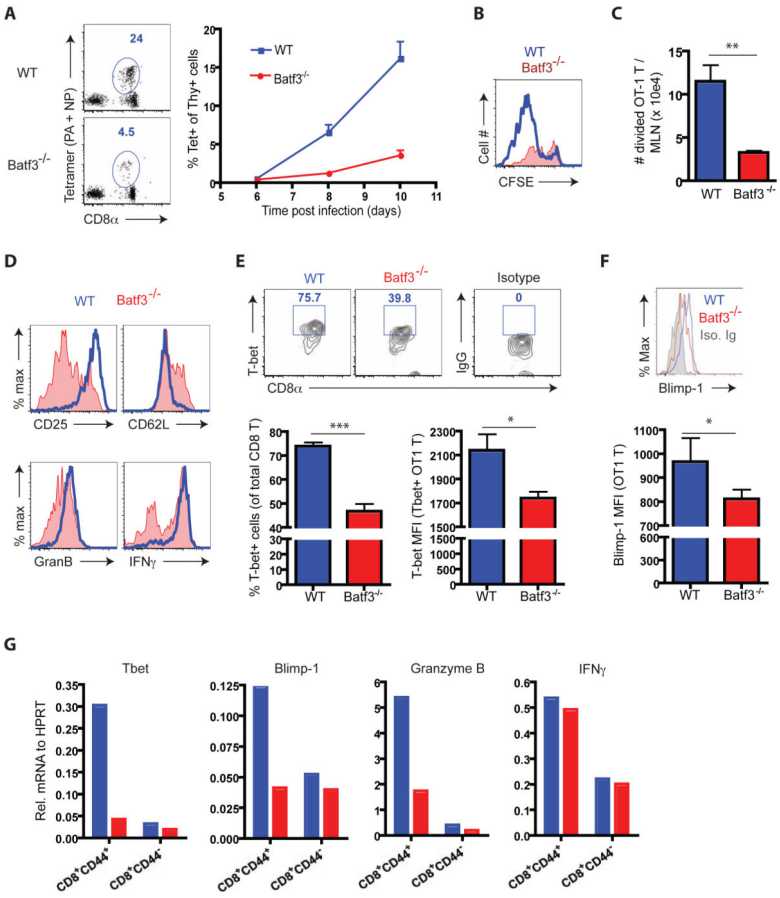

Figure 2.

Egress and initial activation of CD8$^+$ T cells in the DLN of *Batf3*$^{-/-}$ mice. (A) Tet$^+$ CD8 T cells in the circulation of infected *Batf3*$^{-/-}$ and B6 mice were enumerated over time. A rep. FACS plot evaluated at d11 p.i. is shown (n = 8 – 10). (B and C) Congenic mice that had received CFSE labeled OT1 cells (Thy1.1) were infected with IAV-OT1. Division (CFSE dilution) (B) and accumulation of divided (CFSE^{low}) (C) OT1 cells in the DLN were measured at d3.5 p.i. (n > 5). (D – F) At d3.5 p.i., divided OT1 cells in the DLN were examined for surface marker and Granzyme B expression directly *ex vivo*, and IFN**γ** expression after ex vivo cognate peptide restimulation (D), T-bet (E) and Blimp-1 (F) protein expression by flow cytometry (n = 4 - 6). (G) Gene expression profiles of endogenous CD8 T cells activated in the WT (blue) or *Batf3*$^{-/-}$ (red) mice. At d5 p.i., activated (CD44^{hi}) and naïve (CD44$^{lo/-}$) CD8$^+$ T cells were sorted from the DLN of infected mice. *T-bet*, *Blimp-1*, *Granzyme B* and *IFN**γ*** gene expression was evaluated in total mRNA. Data in G represent at least two ind. expts. of cells from pools of 3 - 5 mice prior to sorting. See also Figure S2.

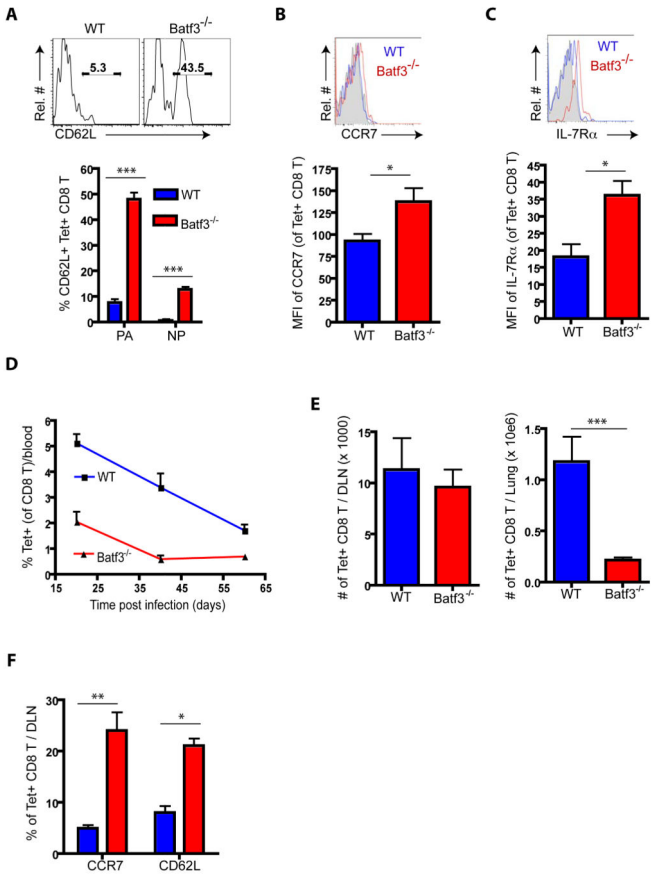

Figure 3.

CD8$^+$ T cells differentiated in the absence of CD103$^+$ RDC exhibit central memory-like T cell properties. (A - C) At > d60 p.i., circulating specific CD8$^+$ T cells in the blood of recovered mice were analyzed for their surface expression of CD62L (A), CCR7 (B) and IL-7RαC - D and E) Frequency of Tet$^+$ CD8$^+$ T cells in the circulation over time (**D**), and in the DLN (left panel in E) and lung (right panel in E) at d65 p.i. (F) The frequency of CD62L^{hi} or CCR7^{hi} CD8$^+$ T cells was measured in the DLN of recovered WT (blue) and *Batf3*$^{-/-}$ (red) mice at d65 p.i. (n = 5 - 8). See also Figure S3.

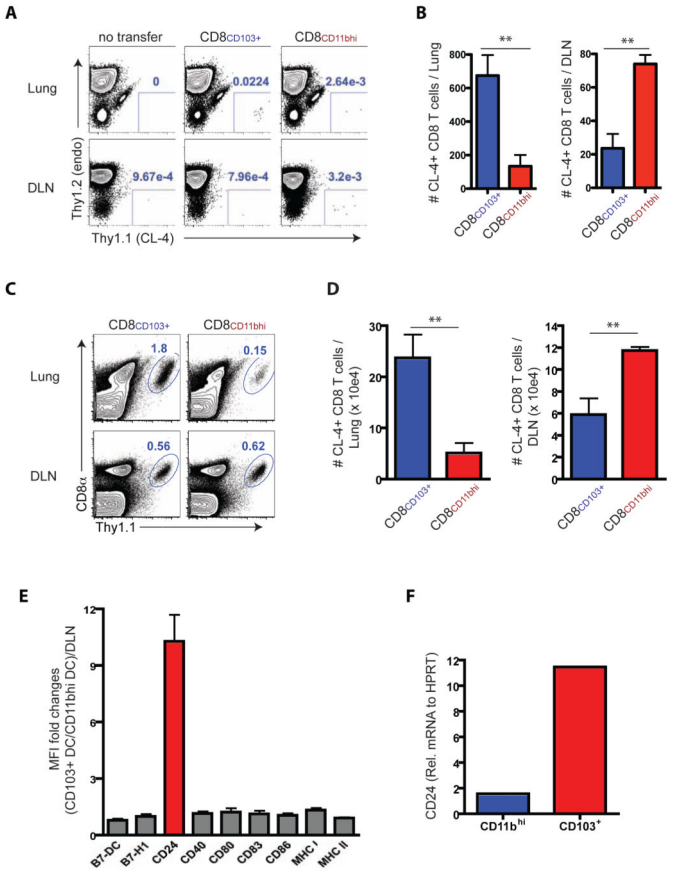

Figure 4.

Trafficking and recall response of CD8$^+$ T cells primed by CD103$^+$ and CD11b^{hi} RDC subsets and costimulatory molecule expression. (A - D) CFSE-labeled naive specific Cl4 cells were stimulated *in vitro* with DLN-derived CD103$^+$ or CD11b^{hi} RDC isolated at d3 p.i. of PR/8 IAV infected mice (from n = 15 – 20 donors/sorting). After d4, the CFSE^{low} cells were sorted, and equivalent cell numbers were individually transferred into Thy-mismatched recipient mice. For trafficking analyses, activated Cl4 cells (1×10^4/mouse) were infused into d5 p.i. B/Lee IAV-infected mice and enumerated in the lungs and DLN of the recipients 24 hr p.t. (A and B). To further analyze the trafficking of the Cl4 cells following IAV challenge, *in vitro* activated Cl4 cells were transferred into uninfected recipient mice and maintained in recipients for 7 days prior to infection with A/PR8 IAV. At d8 p.i., responding Cl4 cells in the lungs and DLN of the infected recipients were evaluated (C and D). Data represent at least two ind. expts. with similar results (n = 4 – 6/group). (E) Expression level of markers by the RDC subsets following migration to the DLN is represented as the ratio of MFI of CD103$^+$ RDC relative to the MFI of CD11b^{hi} RDC. (F) CD24 mRNA in total RNA from the sorted CD103$^+$ RDC and CD11b^{hi} RDC isolated from the pooled DLN (from n = 15 – 20 mice/sorting) was analyzed at d3 p.i. Data represent three independent experiments. See also Figure S4.

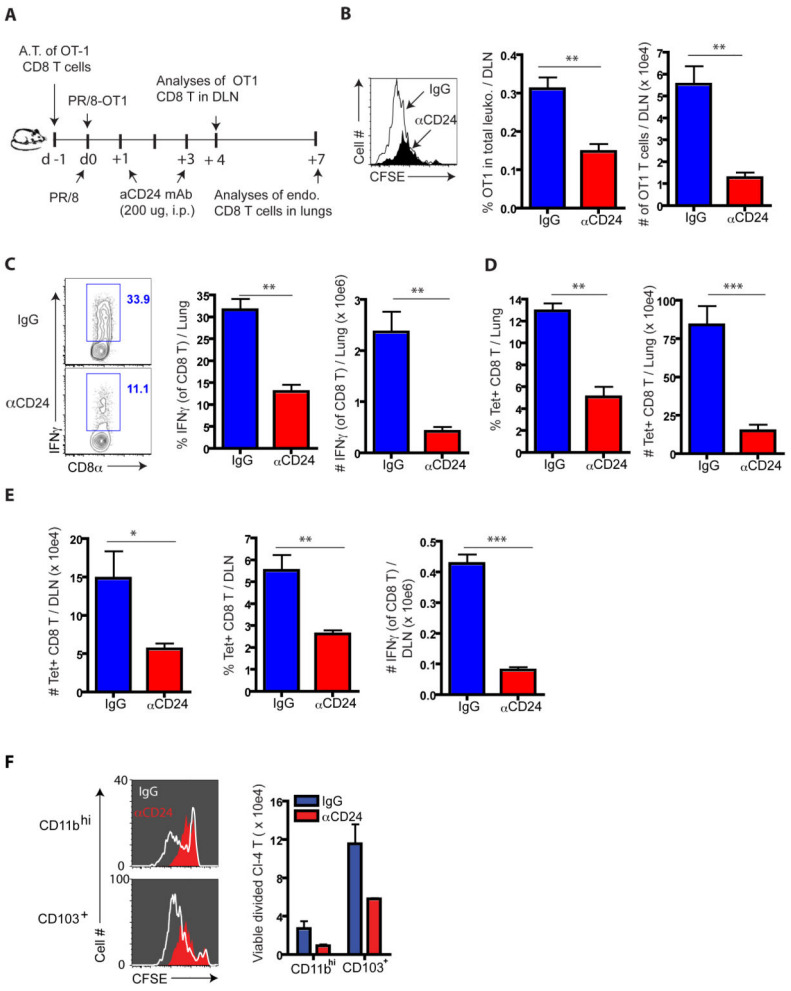

Figure 5.

Impact of CD24 blockade on anti-IAV CD8$^+$ T cell responses *in vivo*. (A) To monitor the effect of CD24 blockade on early events during T cell activation *in vivo*, CFSE-labeled OT1 cells were transferred into B6 WT mice, infected with PR8-OT1 IAV 24 hrs. p.t. These infected recipients were infused i.p. with αCD24 mAb or IgG mAb at both d1 and d3 p.i. (B) Cell division (left panel), the fraction (%) and total numbers of divided OT1 cells (right panels) were enumerated (n = 4 – 5 recipients). (C - E) At d7 p.i., the frequency and total numbers of IAV-responding lung and DLN CD8$^+$ T cells was determined by IFNγ-secretion after infected BMDC restimulation *ex vivo* for 5 hrs (C) and direct *ex vivo* analysis of tet$^+$ (NP and PA) CD8$^+$ T cells in the lungs (D) and DLN (E). Data in C - E represent at least three ind. exps. (n = 4 – 5 mice/group). (F) Requirement of CD24 expressed RDC subsets for full expansion of naïve CD8 T cells. CFSE-labeled naïve Cl4 cells were co-cultured with sorted CD11b^{hi} or CD103$^+$ RDC from d3 p.i DLN (n = 15 – 20 mice/sorting) in the presence (filled in red) or absence (white lines) of αCD24 mAb. At d4, the extent of cell division (left panels) and total divided Cl4 cells (right panel) were examined. Data represent at least three ind. expts. See also Figure S5.

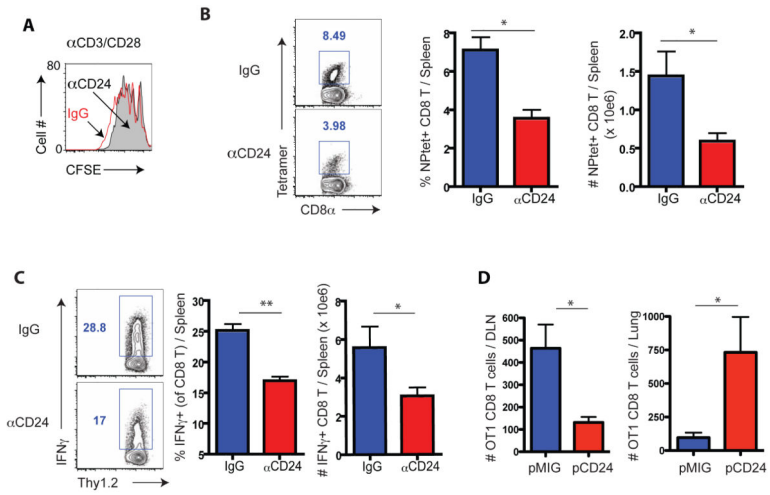

Figure 6.

Elevated CD24 expression by DC enhances $CD8^+$ T cell response and promotes lung homing. (A) Effect of *in vitro* CD24 blockade on αCD3-CD28 Ab-stimulated proliferation of dye labeled Cl4 cells or polyclonal $CD8^+$ T cells (data not shown) as determined by CFSE dilution at d3 of culture. Data is a rep. of three ind. expts. (B and C) IAV-infected BMDC were treated with blocking CD24 mAb prior to transfer into naïve mice. At d7 post infected BMDC transfer, the frequency and total number of tet^+ $CD8^+$ T cells (B) and IFNγ secreting $CD8^+$ T cells following *ex vivo* peptide re-stimulation (C) in the spleens were determined. (D) BMDC over-expressing CD24 by retrovirus transduction (pCD24; Figures S6 E – F and control vector BMDC) were pulsed with OT1 peptide prior to co-culture with naïve OT1 cells (Thy1.1) for 4 days. Activated OT1 cells (5×10^4/mouse) were then transferred into d5 p.i. WT IAV-infected mice (Thy1.2). Accumulation of OT1 cells in the lungs and DLN was evaluated 24 hr later. Data in B - D represent at least three ind. Exps (n = 4 – 5 mice/group). See also Figure S6.

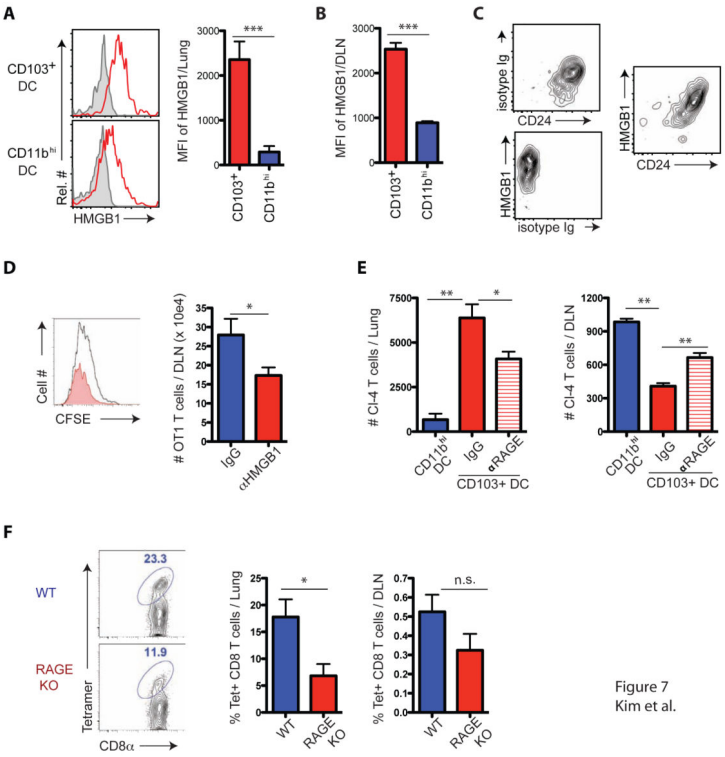

Figure 7.

CD24 controls naïve CD8$^+$ T cell fate decision via RAGE engagement. (A - C) RDC subsets isolated from the lung (A) and DLN (B), respectively, at d3 p.i. were stained for cell-bound HMGB1. Shown are rep. flow cytometric plots (left panels in A) and MFI (right panels in A and B; n = 4 – 5 mice/group). (C) Migrant RDCs in the DLN at d3 p.i. were stained simultaneously with control and mAbs specific for HMGB1 and CD24. Data in **C** are representative of three independent experiments. (D) CFSE-labeled OT1 cells were transferred into naïve WT mice, which were subsequently infected with PR/8-OT1 IAV. αHMGB1 Ab was administered i.n. at d1 and d3, p.i., respectively. OT1 cell proliferation in the DLN was examined at d4 p.i. (n = 4 – 6 mice/group). (E) Naïve Cl4 cells were co-cultured for 4 days with DLN derived CD103$^+$ RDC in the presence or absence of αRAGE Ab. Activated Cl4 cells (5 × 10^4/mouse) were transferred into d6 p.i., B/Lee infected mice and Cl4 cell accumulation in the lungs and DLN was evaluated 24 hr later (n = 4 – 5 mice/group). Cl4 cells activated by CD11b^{hi} RDC were used as controls. Data in D and E represent at least two independent experiments. (F) Mixed BM chimeric mice between WT and *Ager*$^{-/-}$ marrows (1:1) were generated and infected with PR/8. IAV-specific CD45 congenic memory CD8$^+$ T cells were identified in the lungs and DLN (left panels) and enumerated (right panels) at d60 p.i. Data represent at least two ind. expts. (n = 4 – 6/expt). See also Figure S7.